THE STABILITY ENHANCEMENT OF A DFIG-BASED WIND TURBINE GENERATOR CONNECTED TO AN INFINITE BUS USING A PI CONTROLLER

Nguyen Thi Ha

University of Science and Technology, The University of Danang; nthadht@gmail.com

Abstract - This paper presents the design steps and design results of a proportional-integral (PI) controller that can be used to enhance the damping of the electromechanical oscillations of a doubly-fed induction generator (DFIG)-based wind turbine generator (WTG) connected to an infinite bus. The proposed PI controller is designed based on a pole-assignment method that can render adequate damping characteristics to the system under study. A time-domain approach based on nonlinear-system simulations subject to a three-phase short-circuit fault at the infinite bus is performed. The simulation results show that the proposed PI controller is effective on mitigating generator oscillations and offers better damping characteristics to the studied WTG under different operating conditions.

Key words - doubly-fed induction generator; proportional-integral controller; wind turbine generator; damping controller.

1. Introduction

With global environmental problems and the shortage of fossil fuels, the demand of renewable energy is increasing day by day. Among the renewable energy technologies being vigorously developed, the wind turbine technology has been undergoing a dramatic development and now becomes the world's fastest growing energy source [1]. The dramatic increase in the penetration level of the wind power generation into the power system as a serious power source has received considerable attention. Currently, the most widely used commercialized wind-energy conversion system in the world is a variable-speed wind turbine (VSWT) coupled to the rotor of a DFIG through a gearbox. Such configuration can decouple the VSWT-DFIG set from the power grid via the use of power-electronics converters as an interface. The induction generator, which was the most common choice for wind generators before DFIG, can deliver the generated power to the connected power system when its stator windings are directly connected to the power grid and its rotational speed is higher than the synchronous speed. The indirect connection between the VSWT-DFIG set and the power system raises the problem of lacking the damping to suppress power-system oscillations. To maintain the small-signal stability of the power system, effective damping to damp machine oscillations is generally required. With the integration of high-capacity wind power units to power systems, the damping from these conventional power plants may not be sufficient to damp the power-system oscillations within a stability margin. It is desired that the VSWT-DFIG set can also offer adequate damping to power-system oscillations; thus, more wind- energy conversion systems can be extensively integrated to electric power networks.

Among different wind-energy power-generation technologies, the employment of VSWT-GB-DFIG sets with low-cost smaller-capacity power converters located at rotor-winding circuits of the DFIGs for power generation can obtain higher operating efficiency [2-5]. It can also be considered that DFIGs are one of the most commonly used wind generators in wind energy-conversion systems nowadays as they can offer various significant advantages such as the decouple control of active power and reactive power, maximum power-point tracking characteristics, etc.

Based on the above mentioned analysis, this paper illustrates the design produces of a proportional-integral controller that can be improve the damping of the electromechanical oscillations for a DFIG-based WTG connected to an infinite bus.

2. System configuration and mathematical models

The configuration of the studied VSWT-GB-DFIG system connected to an infinite bus is shown in Figure 1. The wind DFIG transforms the input wind turbine power P_{mw} into electrical power. The generated stator power P_{sw} is always positive while the rotor power P_{rw} can be either positive or negative due to the presence of the back-to-back power converter. This allows the wind DFIG to operate under both sub- and super-synchronous speeds [6].

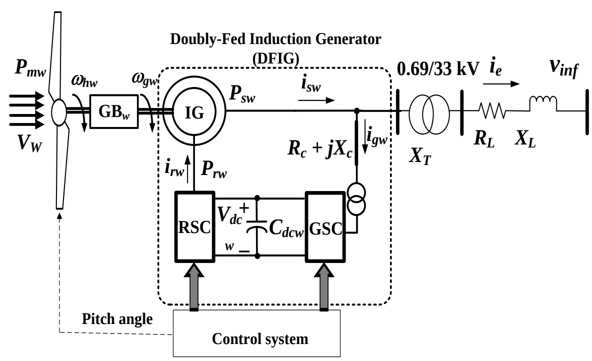

Figure 1. *Configuration of the studied DFIG-based wind turbine generator connected to an infinite bus*

2.1. Model of Variable-Speed Wind Turbine

Wind turbine converts the kinetic energy existed in the wind into mechanical energy. The mechanical power extracted from the VSWTis given by [7].

$$P_{mw} = \frac{1}{2}\rho_w \cdot A_{rw} \cdot V_W^3 \cdot C_{pw}(\lambda_w, \beta_w) \qquad (1)$$

Where ρ_w is the air density (kg/m^3), A_{rw} is the blade impact area (m^2), V_W is the wind speed (m/s), and C_{pw} is the dimensionless power coefficient of the WT. The power coefficient C_{pw} can be written by [8]

$$C_{pw}(\psi_{kw}, \beta_w) = c_1\left(\frac{c_2}{\psi_{kw}} - c_3 \cdot \beta_w - c_4 \cdot \beta_w^{c_5} - c_6\right)\exp\left(-\frac{c_7}{\psi_{kw}}\right) \qquad (2)$$

in which $$\frac{1}{\psi_{kw}} = \frac{1}{\lambda_w + c_8 \cdot \beta_w} - \frac{c_9}{\beta_w^{\ 3} + 1} \quad (3)$$

$$\lambda_w = \frac{R_{bw} \cdot \omega_{bw}}{V_W} \quad (4)$$

Where ω_{hw} is the blade angular speed (rad/s), R_{bw} is the blade radius (m), λ_w is the tip speed ratio, β_w is blade pitchangle (degrees), and c_1-c_9 are the power coefficients of the studied VSWT.

2.2. Mass-Spring-Damper Model

The drive train comprises VSWT, GB, shafts, and the other mechanical components of the VSWT. In power system stability studies, the drive train of a VSWT is usually represented by a simplified reduced-order two-mass model whose block diagram is shown in Figure 2. In Figure 2, T and Gr epresent the mass of the VSWT and the rotor mass of the wind DFIG, respectively while K_{hgw} and D_{hgw} stands for the stiffness and damping between T and G, respectively.

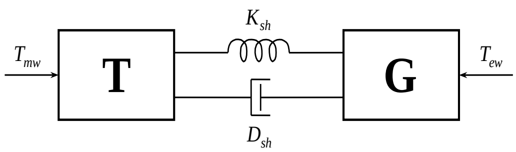

Figure 2. *Simplified reduced-ordertwo-mass model of the VSWT coupled to the wind DFIGURE*

The dynamics of the two-mass drive train model shown in Figure 2 can be expressed by the following per-unit (pu) differential equations [9]

$$(2H_{tw})p(\omega_{tw}) = T_{mw} - K_{hgw}\theta_{tw} - D_{hgw}\omega_b(\omega_{tw} - \omega_r) \quad (5)$$

$$p(\theta_{tw}) = \omega_b(\omega_{tw} - \omega_r) \quad (6)$$

$$(2H_{gw})p(\omega_r) = K_{hgw}\theta_{tw} + D_{hgw}\omega_b(\omega_{tw} - \omega_r) - T_{ew} \quad (7)$$

where p is adifferential operator with respect to time t ($p = d/dt$); ω_{tw} is the purotational speed of the VSWT; ω_r is the purotational speed of the wind DFIG; θ_{tw} is the shaft twist angle between VSWT and DFIG (rad); H_{tw} and H_{gw} are the puinertias of the VSWT and the DFIG (s), respectively; K_{hgw} is the pushaft stiffness coefficient (pu/elec. rad); D_{hgw} is the pushaft damping coefficient (pu·s/elec. rad); T_{ew} is the puelectromagnetic torque of the wind DFIG; and T_{mw} is the pumechanical input torque that can be derived from (1) as $T_{mw} = P_{mw}/\omega_t$.

2.3. Model of doubly-fed induction generator

For the DFIG-based wind turbine shown in Figure 1, the stator windings are directly connected to the low-voltage side of the 0.69/33-kV step-up transformer while the rotor windings are connected to the same 0.69-kV side through a RSC, a DC link, a GSC, a step-up transformer, and a connection line. For the normal operation of a wind DFIG, the input AC-side voltages of the RSC and the GSC can be effectively controlled to achieve simultaneous active-power and reactive-power modulation. The detailed operation of the RSC and GSC can be referred to [10].

Neglecting the power losses in the RSC and GSC, the power balance equation for the back-to-back converter shown in Figure 1 can be written as

$$P_{rw} = P_{gw} - P_{dcw} \quad (8)$$

Where P_{rw}, P_{gw}, and P_{dcw} are the active power at the AC terminals of the RSC, the active power at the AC terminals of the GSC, and the active power at the DC-link, respectively. The three powers P_{rw}, P_{gw}, and P_{dcw} can be expressed respectively by

$$P_{rw} = v_{drw}\, i_{drw} + v_{qrw}\, i_{qrw} \quad (9)$$

$$P_{gw} = v_{dgw}\, i_{dgw} + v_{qgw}\, i_{qgw} \quad (10)$$

$$P_{dcw} = v_{dcw} i_{dcw} = v_{dcw} \cdot [C_{dcw}\, p(v_{dcw})] \quad (11)$$

Substituting (9)-(11) into (8), the dynamic equation of the DClink can be obtained as

$$(C_{dcw} v_{dcw})\, p(v_{dcw}) = v_{dgw}\, i_{dgw} + v_{qgw}\, i_{qgw} - v_{drw}\, i_{drw} - v_{qrw}\, i_{qrw} \quad (12)$$

where i_{qrw} and i_{drw} are the pu$q$- and d-axis currents of the RSC, respectively; i_{qgw} and i_{dgw} are the pu$q$- and d-axis currents of the GSC, respectively; v_{qrw} and v_{drw} are the pu$q$- and d-axis AC-side voltages of the RSC, respectively; v_{qgw} and v_{dgw} are the pu$q$- and d-axis AC-side voltages of the GSC, respectively; and v_{dcw} is the pu DC-link voltage.

2.4. RSC controller

Figure 3 shows the control block diagram of the RSC. The RSC controller is used to control the electromagnetic torque of the DFIG to follow an optimal torque-speed characteristic in order to maintain the terminal voltage of the DFIG at the reference value. This controller is similar to the one in [11], where the reactive power is controlled instead of the terminal voltage of the DFIGURE

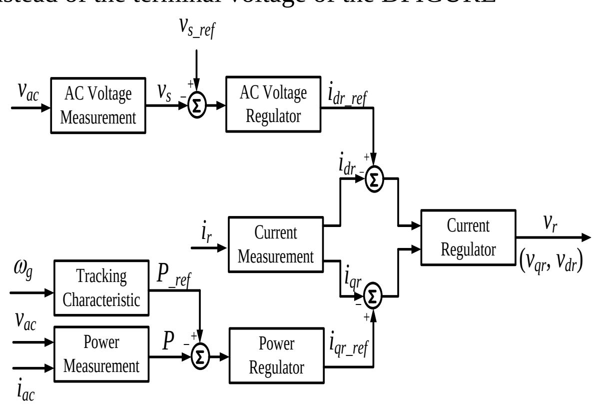

Figure 3. *Control block diagram for the RSC of the wind DFIG*

Table 1. *Eigenvalues (rad/s) of the studied system without and with pi controller*

Modes		Without PI controller			With PI controller		
		Eigenvalues	ζ	***f*** (Hz)	Eigenvalues	ζ	***f*** (Hz)
$\Lambda_{1,2}$	v_{qs},v_{ds}	-13.497 ± j47918	0.000282	7626.5	-13.497 ± j47918	0.000282	7626.5
$\Lambda_{3,4}$		-13.601 ± j47164	0.000288	7506.5	-13.601 ± j47164	0.000288	7506.5

$\Lambda_{5,6}$	i_{qs}, i_{ds}	$-28.601 \pm j410.4$	0.069523	65.159	$-28.601 \pm j410.4$	0.069523	65.159
$\Lambda_{7,8}$		$-6.8501 \pm j375.68$	0.018230	59.781	$-6.8501 \pm j375.68$	0.018230	59.781
$\Lambda_{9,10}$	i_{qs},i_{qr}	$-28.512 \pm j384.63$	0.073924	61.049	$-28.512 \pm j384.63$	0.073924	61.049
$\Lambda_{11,12}$		$-5.7373 \pm j77.123$	0.074209	12.241	$-5.7373 \pm j77.123$	0.074209	12.241
$\Lambda_{13,14}$	i_{dr}, i_{ds}	$-5.7103 \pm j38.281$	0.147730	6.0257	$-5.7103 \pm j38.281$	0.147730	6.0257
$\Lambda_{15,16}$		$-3.5133 \pm j32.648$	0.106920	5.1661	$-3.5133 \pm j32.648$	0.106920	5.1661
$\Lambda_{17,18}$	θ_{hg}	**$-1.8692 \pm j10.434$**	**0.1768**	**1.6341**	**$-3.0 \pm j10.0^{*}$**	**0.28735**	**1.5244**

* denotes the assigned eigenvalue.

2.5. GSC controller

The GSC controller aims to maintain the DC-link voltage constant and control the reactive power exchanged between the GSC and the grid. For the minimum converter rating as assumed in this paper, the GSC is controlled to operate at a unity power factor and, hence, exchanges only active power with the grid. In order to achieve the decoupled control of active and reactive power flowing between the GSC and the grid, the stator-voltage-oriented synchronous reference frame with its *d*-axis aligning the stator voltage vector is adopted [8]. The control block diagram of the GSC controller is shown in Figure 4.

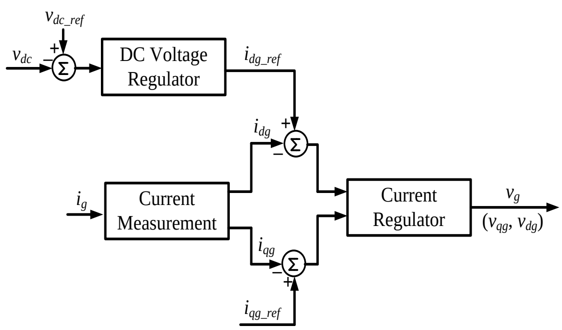

Figure 4. *Control block diagram for the GSC of the wind DFIGURE*

3. Design PI damping controller

Figure 5 shows the control block diagram of the *d*-axis rotor-winding voltage of the wind DFIGURE The terminal voltage of the DFIG $v_s$is compared with its reference value v_{s_ref} to generate the deviation of the *d*-axis rotor-winding reference current Δi_{dr_ref} though a first-order lag. The value of Δi_{dr_ref} is added to its nominal value i_{dr_ref0} to obtain the *d*-axis rotor-winding reference current i_{dr_ref}. The *d*-axis rotor-winding current i_{dr} is compared with i_{dr_ref} to obtain the deviation of the *d*-axis rotor-winding voltage reference Δv_{dr_ref} through a first-order lag. The value of Δv_{dr_ref} is then added to its nominal value v_{dr_ref0} to obtain the required *d*-axis rotor-winding voltage v_{dr}.

The damping signal v_a at the right bottom part of Figure 5 is used for the damping improvement of the studied DFIG, and this signal can be obtained from the output of a designed PI damping controller.

To design the PI damping controller using $\Delta\omega_r$ as a feedback signal for the studied wind DFIG, the closed-loop characteristic equation of the studied system using Mason's rule is shown as follows:

$$1 + G(s)H(s) = 0 \tag{13}$$

where $G(s)$ is the forward-gain transfer function of the open-loop studied system and it is from the input signal v_a to the output signal $\Delta\omega_r$; $H(s)$ is the transfer function of the PI damping controller that is from the output signal $\Delta\omega_r$ to the input signal v_a, and s is one of the eigenvalues or poles of the closed-loop system.

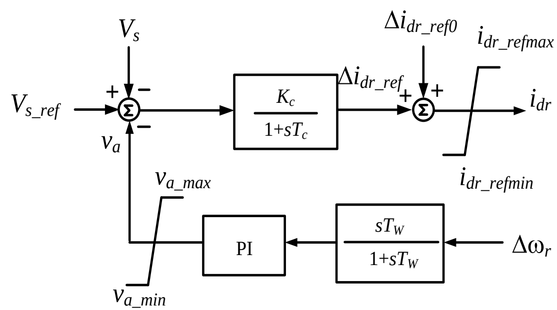

Figure 5. *Control block diagram of the d-axis rotor-winding voltage of the studied wind DFIGURE*

The nonlinear equations of the studied system are first linearized around a selected steady-state operating point to obtain a set of linearized system dynamic equations which can be expressed in the matrix form as follows:

$$p\mathbf{X}(t) = \mathbf{AX}(t) + \mathbf{BU}(t) \tag{14}$$

$$\mathbf{Y}(t) = \mathbf{CX}(t) + \mathbf{DU}(t) \tag{15}$$

Where X(t) is the state vector, Y(t) is the output vector, U(t) is the input vector, A is the state matrix, B is the input matrix, C is the output matrix, and D is the (feedforward) matrix while A, B, C, and D are all constant matrices of appropriate dimensions. The eigenvalues of the open-loop system can be determined from the following characteristic equation:

$$\det(s\mathbf{I} - \mathbf{A}) = 0 \tag{16}$$

Where I is an identity matrix with the same dimensionsas A while the values of s satisfying (16) are the eigenvalues of the open-loop studied system. By taking Laplace transformation on both sides of (14)-(15), the state-space equations in frequency domain can be obtained as

$$s\mathbf{X}(s) = \mathbf{AX}(s) + \mathbf{BU}(s) \tag{17}$$

$$\mathbf{Y}(s) = \mathbf{CX}(s) + \mathbf{DU}(s) \tag{18}$$

Using (17) to eliminate $\mathbf{X}(s)$ in (18), it yields

$$\mathbf{Y}(s) = \{\mathbf{C}(s\mathbf{I} - \mathbf{A})^{-1}\mathbf{B} + \mathbf{D}\}\mathbf{U}(s) = G(s)\mathbf{U}(s) \tag{19}$$

Where $G(s)$ is the forward-gain of the open-loop system in the frequency domain and it is the ratio of output signal $\mathbf{Y}(s)$ to the input signal $\mathbf{U}(s)$:

$$G(s) = \frac{\mathbf{Y}(s)}{\mathbf{U}(s)} = \mathbf{C}(s\mathbf{I} - \mathbf{A})^{-1}\mathbf{B} + \mathbf{D} \quad (20)$$

The transfer function $H(s)$ in Figure 5 can be expressed by

$$H(s) = \frac{\mathbf{U}(s)}{\mathbf{Y}(s)} = \frac{v_a(s)}{\Delta\omega_r(s)} = \frac{sT_W}{1+sT_W}(K_P + \frac{K_I}{s}) \quad (21)$$

Substituting $G(s)$ and $H(s)$ into Mason's rule in (16) and extending, it yields

$$G(s)sT_W K_P + G(s)T_W K_I + sT_W = -1 \quad (22)$$

As mentioned before, the design task is to find the parameters T_W, K_P, and K_I. The washout-term time constant T_W is not critical and it can be pre-specified [12-13] while K_P and K_I are two unknown parameters for assigning only one desired complex-conjugated pole. The washout-term time constant T_W of 0.1s is properly chosen in this paper. The eigenvalues of the studied system without and with the PI controller at the operating point specified are listed in the third and sixth columns of Table 1, respectively. In Table 1, ζ denotes the damping ratio andfrepresents the oscillation frequency in Hz. The assigned eigenvalues are Λ17,18 = -3.0 ± j10.0rad/s while the parameters of the designed PI controller are: K_P = -21.02, K_I = 20.74, and T_W = 0.1 s.

4. Time-domain Simulations

The main objective of this section is to demonstrate the effectiveness of the designed PI damping controller on enhancing dynamic stability of the studied system subject to a three-phase short-circuit fault at the infinite bus.

The Matlab/ Simulink is used to design the PI controller and simulate the transient responses of the studied system. Figure 6 plots the comparative transient responses of the studied DFIG-based WTG without and withthe designed PI controller when a three-phase short-circuit fault is suddenly applied to the infinite bus at t = 1 s and it is cleared at t = 1.1 s.

It is obviously seen from the comparative transient responses shown in Figure 6 that transient responses of the studied system without the designed PI controller have larger oscillations. On the other hand, the oscillations of transient responses of the studied system can be effectively mitigated by the proposed control scheme.

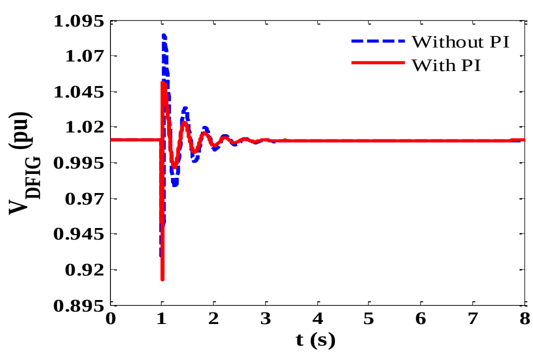

(a) V_{DFIG}

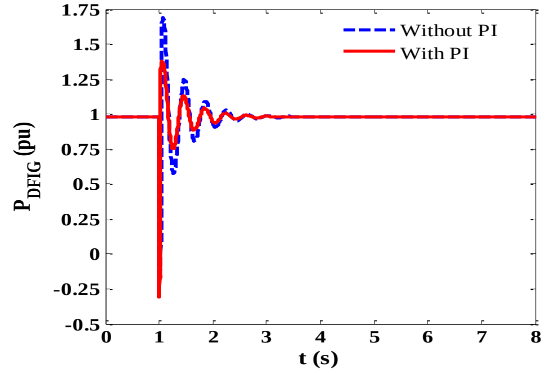

(b) P_{DFIG}

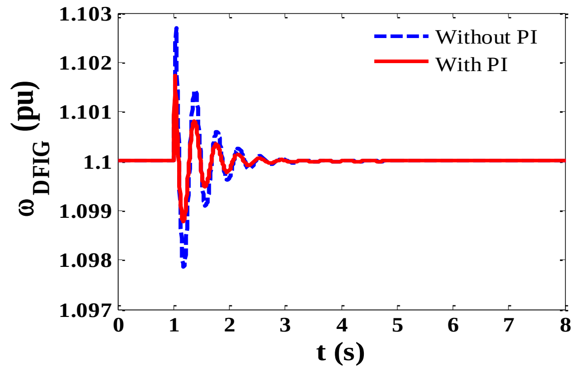

(c) ω_{DFIG}

Figure 6. *Transient responses of the studied system with and without PI controller subject to a three-phase short-circuit fault at the infinite bus: (a) terminal voltage of DFIGURE, (b) active power of DFIGURE, (c) rotor speed of DFIGURE*

5. Conclusion

In this paper, the design of PI controller for the damping enhancement of a DFIG-based WTG subject to a severe power-system fault has been investigated. The pole-assignment algorithm has been used to find the parameters of the proposed PI damping controllers. The effectiveness of the proposed PI on improving the damping of the studied WTG has been demonstrated under a severe three-phase short-circuit fault. The simulation results have shown that the proposed control scheme can effectively damp the oscillations of the studied DFIG-based WTG under a three-phase short-circuit fault.

REFERENCES

[1] U. Bossel, "On the way to a sustainable energy future", in *Proc. 27th International Telecommunications Conference (INTELEC)*, Berlin, Germany, Sep. 18-22, 2005, pp. 659-668.

[2] R. Pena, J. C. Clare, and G. M. Asher, "Doubly fed induction generator using back-to-back PWM converters and its application to variable speed wind-energy generation", *IEE Proceedings - Electric Power Applications*, vol. 143, no. 3, May 1996, pp. 231-241.

[3] J. B. Ekanayake, L. Holdsworth, X. Wu, and N. Jenkins, "Dynamic modeling of doubly fed induction generator wind turbines", *IEEE Trans. Power Systems*, vol. 18, no. 2, May 2003, pp. 803-809.

[4] L. Shi, Z. Xu, J. Hao, and Y. Ni, "Modeling analysis of transient stability simulation with high penetration of grid-connected wind farms of DFIG type", *Wind Energy*, vol. 10, no. 4, Mar. 2007, pp. 303-320.

[5] O. Anaya-Lara, F. M. Hughes, N. Jenkins, and G. Strbac, "Rotor flux magnitude and angle control strategy for doubly fed induction generators", *Wind Energy*, vol. 9, no. 5, Sep./Oct. 2006, pp. 479-495.

[6] R. S. Pena, "Vector control strategies for a doubly-fed induction

generator driven by a wind turbine", Ph.D. dissertation, Univ. Nottingham, Nottingham, U.K., 1996.

[7] I. Erlich, J. Kretschmann, J. Fortmann, S. Mueller-Englhardt, and H. Wrede, "Modeling of wind turbines based on doubly-fed induction generators for power system stability studies", *IEEE Trans. Power Systems*, vol. 22, no. 3, Aug. 2007, pp. 909-919.

[8] L. Yang, G. Y. Yang, Z. Xu, Z. Y. Dong, K. P. Wong, and X. Ma, "Optimal controller design of a doubly-fed induction generator wind turbine system for small signal stability enhancement", *IET Generation, Transmission & Distribution*, vol. 4, no. 5, May 2010, pp. 579-597.

[9] F. Mei and B. Pal, "Modal analysis of grid-connected doubly fed induction generators", *IEEE Trans. Energy Conversion*, vol. 22, no. 3, Sep. 2007, pp. 728-736.

[10] L. Wang, K.-H.Wang, W.-J.Lee, and Z. Chen, "Dynamic stability analysis of a DFIG-based offshore wind farm connected to a power grid through an HVDC link", *IEEE Trans. Power Systems*, vol. 26, no. 3, Aug. 2011, pp. 1501-1510.

[11] B. C. Pal and F. Mei, "Modeling adequacy of the doubly fed induction generator for small-signal stability studies in power systems", *IET Renewable Power Generation*, vol. 2, no. 3, Sep. 2008, pp. 181-190.

[12] S. Panda, N. P. Padhy, and R. N. Patel, "Power-system stability improvement by PSO optimized SSSC-based damping controller", *Electric Power Components and Systems*, vol. 36, no. 5, Apr. 2008, pp. 468-490.

[13] L. Wang, S.-S.Chen, W.-J. Lee, and Z. Chen, "Dynamic stability enhancement and power flow control of a hybrid wind and marine-current farm using SMES", *IEEE Trans. Energy Conversion*, vol. 24, no. 3, Sep. 2009, pp. 626-639.

(The Board of Editors received the paper on 10/23/2014, its review was completed on 10/31/2014)